Eur. Phys. J. B **7**, 619–625 (1999)

THE EUROPEAN PHYSICAL JOURNAL B

EDP Sciences

Time distribution and loss of scaling in granular flow*

B. Tadić[a]

Jožef Stefan Institute, P.O. Box 3000, 1001-Ljubljana, Slovenia

Received: 29 May 1998 / Revised: 8 September 1998 / Accepted: 10 September 1998

Abstract. Two cellular automata models with directed mass flow and internal time scales are studied by numerical simulations. Relaxation rules are a combination of probabilistic critical height (probability of toppling p) and deterministic critical slope processes with internal correlation time t_c equal to the avalanche lifetime, in model A, and $t_c \equiv 1$, in model B. In both cases nonuniversal scaling properties of avalanche distributions are found for $p \geq p^\star$, where $p^\star$ is related to directed percolation threshold in $d = 3$. Distributions of avalanche durations for $p \geq p^\star$ are studied in detail, exhibiting multifractal scaling behavior in model A, and finite size scaling behavior in model B, and scaling exponents are determined as a function of p. At $p = p^\star$ a phase transition to noncritical steady state occurs. Due to difference in the relaxation mechanisms, avalanche statistics at $p^\star$ approaches the parity conserving universality class in model A, and the mean-field universality class in model B. We also estimate roughness exponent at the transition.

PACS. 81.05.Rm Porous materials; granular materials – 64.60.Lx Self-organized criticality; avalanche effect – 02.60.Cb Numerical simulation; solution of equations

1 Introduction

Dynamics of granular materials represents an important practical and theoretical problem. A new theoretical approach to the problem of driven granular flow has been initiated in the past few years [1], which is motivated by the observed scaling behavior both in the laboratory granular piles and in natural landslides [2–8]. It has been recognized that the collective dynamics of grains may lead to a self-organized critical (SOC) states [1], characterized by scaling properties of sandslides (avalanches). Moreover, dynamics may depend on various parameters, such as dimension and mass of individual grains and quality of their contact surfaces, and on the external conditions. By varying some of these parameters in a controlled manner, steady states with different characteristics are reached, and a phase transition to a steady state with no long-range correlations occurs when a parameter is varied through certain critical value [6].

Various cellular automata models have been introduced so far to mimic stochastic variations in the conditions of toppling [9–14]. One-dimensional rice-pile automata with stochastic critical slope rules have been useful in understanding transport properties of rice piles [9]. Relaxation rules in these models are a kind of branching processes with internal stochasticity. In two dimensions, two models studied in references [13,14] utilize mixed dynamic critical slope (CS) and critical height (CH) rules, motivated by the observed nonuniversality of the emergent critical states in natural landslides (for a recent review see Refs. [15,16]).

In the present work we extend the study of the models of references [14,13], which we term model A and B, respectively. In these models stochastic toppling by the CH mechanism is controlled by an external parameter – probability of toppling p, which can be attributed to variations in the external conditions (*e.g.*, wetting), or by internal kinetic friction, determined globally by the quality of contact surfaces between grains. In contrast to rice-pile models of references [9,12], the present models are more appropriate for the evolution of landscape, in which a variety of erosion mechanisms might be simultaneously active.

Two types of triggering mechanisms of landslides are recognized in the literature [16,17,14]: (i) soil moisture, which is controlled by rainfall and water level, and (ii) ground motion, which influences slope variation. The local shear stress threshold may depend on both slope angle and soil properties. We assume that these triggering mechanisms are dynamically correlated. By wetting diffusion probability is lowered and grains stick together, thus building up local heights. However, when the *difference* between heights at neighboring sites exceeds certain limit, the slope mechanism becomes activated.

A simplified picture of the natural mechanisms of erosion is taken into account by combined relaxation rules for the height transport on a two-dimensional square lattice, as follows: if at a site (i, j) local height $h(i, j) \geq h_c$, then

* This paper is dedicated to Professor Franz Schwabl on the occasion of his 60th birthday.

[a] e-mail: `bosilijka.tadic@ijs.si`

the site relaxes *with probability* p as $h(i,j) \to h(i,j) - 2$; $h(i+1, j_\pm) \to h(i+1, j_\pm) + 1$. If for finite p some of the local slopes $\sigma_\pm(i,j) \equiv h(i,j) - h(i+1, j_\pm) \geq \sigma_c$, then the site relaxes with probability *one* by toppling one particle along each unstable slope, repeatedly until all slopes are reduced below σ_c. Here $(i+1, j_\pm)$ are positions of two downward neighbors of the site (i,j) on a square lattice oriented downward, $h_c = 2, \sigma_c = 8$.

The system is driven by adding grain from the outside at a random site along first row and the system is let to relax according to the above rules. Another grain is added when the relaxation process stops. The internal time scale is measured by the number of steps that the relaxation process proceeds on the lattice. At time step $t = 1$ a site at first row topples after added grain from outside. According to the above relaxation rules, one or two grains are toppled from that site, which then appear at one or two downward neighboring sites. Therefore, mass flow is only down. However, an instability may propagate to both downward and upward neighbors of a toppled site (except for the sites on the first row, which have no upward neighbors), thus triggering four new sites as candidates for toppling per each just toppled site. At one time step we update *in parallel* all candidates for toppling. This comprises the usual definition of the time step in cellular automata models.

Since the system builds up unstable sites (with respect to probabilistic CH rule), the above dynamic rules need to be supplemented by an additional rule, which makes the difference between two models. In model A, all sites that are visited by an avalanche at least once are considered as candidates for toppling until the whole instability dies off. In this way a propagating instability has an internal correlation time t_c which is determined by the dynamics itself. In model B, we set $t_c = 1$. Therefore, only sites which are in the neighborhood of active sites at time t may be candidates for toppling in the next time step $t + 1$. It should be stressed that, since an avalanche is extended object, in both models there are many sites which topple simultaneously and which are not neighbors in space. In model B next toppled sites are neighbors only on time scale but not in space, whereas in model A next toppled sites are not necessarily neighbors neither on temporal nor spatial scale. However, all toppled sites are connected *within affected* area in space-time dimensions. In both models particles are added from the outside only on a random site at the first row and leave the system at lower (open) boundary. The mass transport is unidirectional (down). However, since the above rules allow an instability to propagate both forward and backward on a 2-dimensional lattice, and evolve on an internal time scale, both models are essentially (2+1)-dimensional, with extra dimension representing the internal time scale. Differences in the additional relaxation rule lead to different emergent critical states, as explained below.

In Figure 1 two examples of large avalanches in model A (below) and model B (top) are shown for values of the control parameter $p = p^\star$ at the edge of the scaling region ($p^\star \sim 0.4$, see Sect. 4 for discussion). In both models multiplicity of topplings at a site (larger number of topplings is marked by darker gray tone), is induced by the instability propagating back and forth due to nonlocal relaxation rules. In model A number of candidates for toppling at each time step is larger compared to model B, due to internal correlation time typically $t_c \gg 1$, leading to more efficient relaxation of unstable sites. On the other hand, $t_c = 1$ in model B enables building up numerous unstable sites (with respect to CH rule) for low values of $p \sim p^\star$. Therefore huge avalanches with perpendicular extent comparable to the system size (*cf.* Fig. 1 (top)) occur frequently, indicating that the anisotropy of the relaxation events vanishes at $p^\star$.

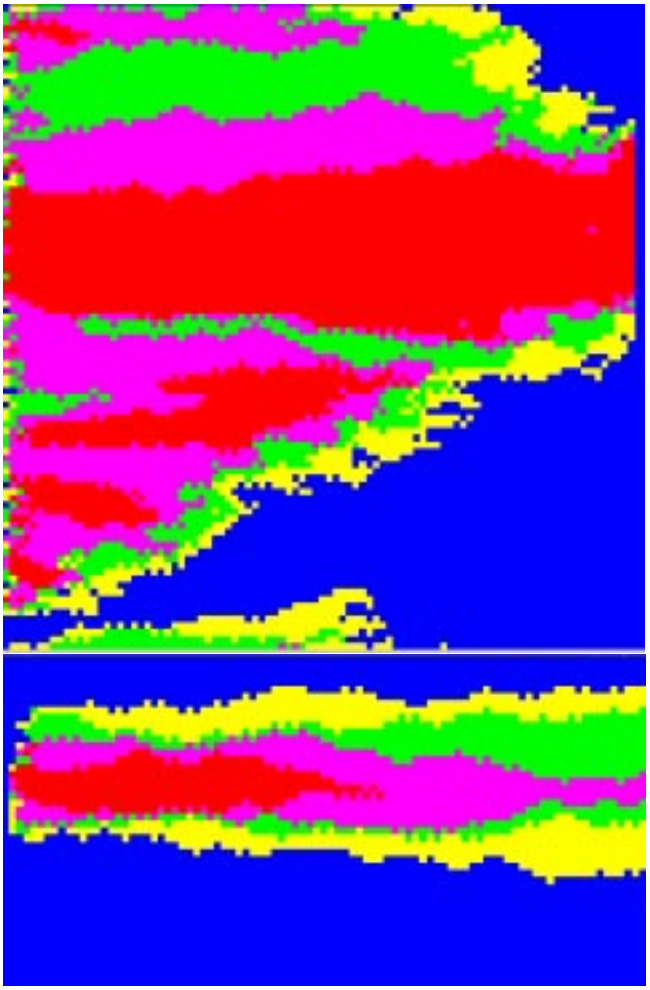

Fig. 1. Two examples of large avalanches running from left to right at $p = p^\star$: in model A (below) and in model B (top). Multiple topplings up to forth order are marked by different degree of gray color.

In the limit $p = 1$ both models reduce to the deterministic directed CH model introduced and solved exactly by Dhar and Ramaswamy in reference [18]. In this limit slopes are restricted to $\sigma_\pm(i,j) \leq 1$, and thus CS rule remains inactive.

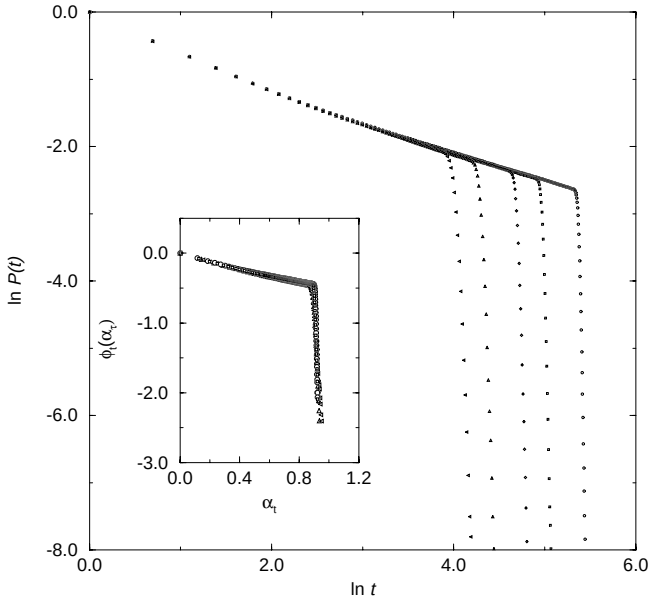

Fig. 2. Double-logarithmic plot of the integrated distribution $P(t)$ *vs.* t for $p = 0.7$ and for various lattice sizes $L = 12$, 24, 48, 96, and 192 (left to right) in model A, obtained by open boundary conditions. Inset: multifractal spectral function $\phi_t(\alpha_t)$ *vs.* α_t. (Fig. 3 from Ref. [14]).

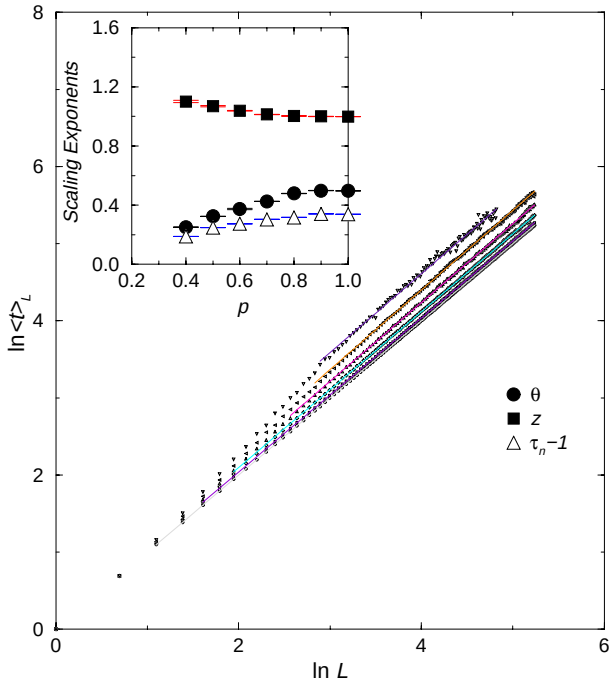

Fig. 3. Average duration time of avalanches of selected length $\langle t \rangle_L$ *vs.* length L for various values of $p = 1$, 0.7, 0.6, 0.5, and 0.4 (bottom to top) in model A. Maximal length equals the system size $L_{max} = 192$, except for $p = 0.4$, where $L_{max} = 128$. Inset: scaling exponents $\theta \equiv \tau_t - 1$, z, and $\tau_n - 1$, defined in the text, *vs.* p in the scaling region.

2 Model A: Multifractal scaling behavior of landslides

Correlation times $t_c > 1$ in model A are motivated by varying toppling conditions after an avalanche commenced, which represents a natural choice in the case of long relaxation times, such as geological evolution of landslides. It has been shown that this type of temporal disorder is a relevant perturbation both for the evolution of landslides [14] and for directed percolation processes [19]. In this model each site develops an individual time scale of activity, which then contributes to the whole event (avalanche). As a consequence, the distribution of avalanche durations $P_A(t, L)$ in the scaling region exhibits *multifractal scaling* properties when the system size L is varied, according to the expression:

$$P_A(t, L) = (L/L_0)^{\phi_t(\alpha_t)};$$
$$\alpha_t \equiv \left(\ln \frac{t}{t_0}\right) \Big/ \left(\ln \frac{L}{L_0}\right). \qquad (1)$$

In Figure 2 the distribution of duration of avalanches is shown for $p = 0.7$ and various lattice sizes. In the inset the spectral function $\phi_t(\alpha_t)$ *vs.* α_t is determined by the scaling plot according to equation (1), with $t_0 = 1/4$ and $L_0 = 1/4$. The integrated distribution of durations exhibits a power-law behavior as $P(t) \sim t^{-(\tau_t - 1)}$ in the entire region $p^\star \leq p < 1$, with the p-dependent exponent $\theta \equiv \tau_t - 1$, which is shown in the inset to Figure 3. Similar nonuniversality with decreasing scaling exponents with the parameter p are found for the distributions of size $D(s) \sim s^{-(\tau_s - 1)}$, and mass of avalanches $D(n) \sim n^{-(\tau_n - 1)}$ (see Ref. [14] for detailed analysis). Slopes of various curves in the main Figure 3 determine the dynamic exponent $z(p)$, which is also shown in the inset to Figure 3. For values of the control parameter p below a critical value $p^\star \approx 0.4$ (see below) the critical steady states are no longer accessible by the dynamics.

3 Model B: Nonuniversal scaling in granular piles

For finite correlation times, *i.e.*, by setting $t_c = 1$, avalanches have in the average a reduced number of topplings per site, compared with model A for the same value of the control parameter p. This leads to a smaller incidence of large avalanches, and thus to increase of the scaling exponents with decreasing probability of toppling p. In Figure 4 the probability distribution of avalanche durations is shown for few values of p in the scaling region. On the other hand, for short correlation times the balance between the CS and CH toppling mechanisms is altered: by lowering p the system builds up heights faster than in the case of model A, and thus the CS mechanism becomes more effective, and eventually prevails at the boundary of the scaling region at $p^\star$. We find numerically that scaling behavior is lost at $p^\star \leq 0.5$ [13]. The scaling behavior for $p^\star \leq p < 1$ is characterized by nonuniversal p-dependent scaling exponents (see inset to Fig. 5 and Ref. [13]).

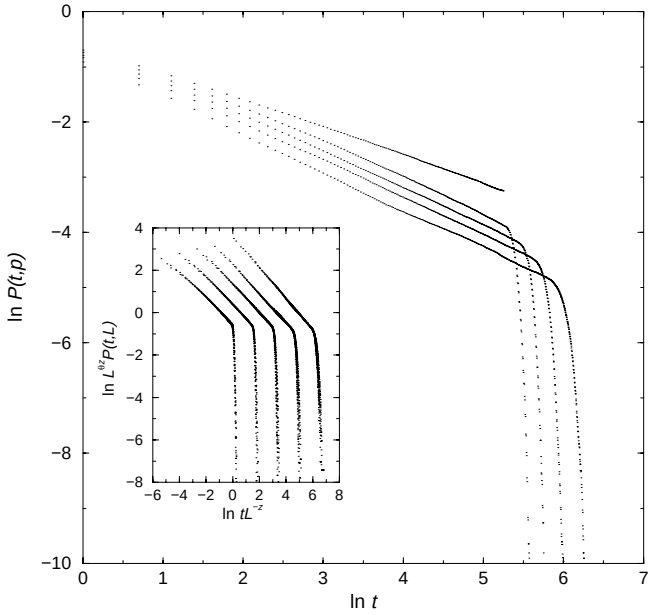

Fig. 4. Double-logarithmic plot of the integrated distribution $P(t)$ *vs.* t for various values of the parameter $p = 1$, 0.8, 0.7, 0.6, and 0.5 (top to bottom) and system size $L = 192$ in model B. Inset: finite size scaling plots for the same values of p as in the main figure (left to right). For each plot three different lattice sizes $L = 48$, 96, and 192 are used. Plots for different values of p are shifted to the right for easier display.

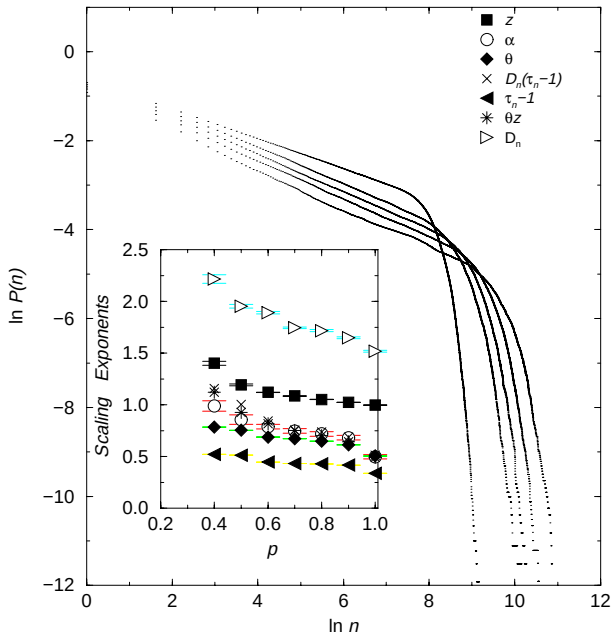

Fig. 5. Double-logarithmic plot of the integrated distribution of mass of avalanche $D(n)$ *vs.* mass n for $L = 192$ and for $p = 1$, 0.8, 0.7, 0.6, and 0.5 (top to bottom) in model B. Inset: scaling exponents $\alpha \equiv \tau_\ell - 1$, $\theta \equiv \tau_t - 1$, and $\tau_n - 1$, fractal dimensions z and D_n, and products $D_n(\tau_n - 1) = z\theta$ plotted against p in the scaling region (see text).

The scaling properties of the distribution of avalanche durations are determined by using the following finite-size scaling form

$$P_B(t, L) \sim L^{-\theta z} \mathcal{P}(tL^{-z}) \; , \qquad (2)$$

where $\theta \equiv \tau_t - 1$ as above, and z is the dynamic exponent, which also depends on p. The scaling plots of $P_B(t, L)$ for various values of p in the scaling region and for three system sizes at each value of p, are shown in the inset to Figure 4. Similar scaling properties are found for the distributions of size and length of avalanches (see Ref. [13] for detailed discussion). In addition to the temporal distribution discussed above, here we also concentrate on the distribution of mass of avalanches, $P_B(n, L)$, satisfying the scaling form $P_B(n, L) \sim n^{\tau_n - 1} \mathcal{Q}(nL^{-D_n})$, where mass n of an avalanche is determined as total number of grains that slide during one avalanche. In Figure 5 the distribution of mass of avalanches is shown for few different values of the parameter p in the scaling region. In the inset to Figure 5 we plot the exponents $\theta(p)$ and $\tau_n(p) - 1$, for duration and mass of avalanches, respectively, and the dynamic exponent $z(p)$, and fractal dimension of mass $D_n(p)$ against p. For $p \geq 0.5$ the following scaling relations are satisfied (*cf.* inset to Fig. 5): $(\tau_n - 1)D_n = z\theta = \alpha$, where $\alpha \equiv \tau_\ell - 1$ is the exponent of length of avalanches, which is determined in reference [13]. The dynamic exponent z which appears in the scaling form (2) can also be determined from slopes of the curves $\langle t \rangle_\ell$ *vs.* ℓ, similar as we have determined it in model A. Obtained values are in a good agreement, within numerical error bars, with those obtained from the scaling plots in Figure 4. Values of the exponents at $p = 0.4$ are taken from the straight sections of the lines representing distributions of duration and mass for smaller system sizes $L \leq 128$. As indicated in the inset to Figure 5, these values do not satisfy scaling relations within error bars, indicating that $p = 0.4$ is already beyond the edge of the scaling region in model B (see discussion in Sect. 4).

4 Universal criticality at the edge of the scaling region

When the control parameter p is varied through a critical value $p^\star$ we find that the scaling behavior of the avalanche distributions is lost, indicating that self-organized critical states are no longer accessible by the dynamics. By numerical simulations of various distributions and applying the appropriate scaling analysis it was shown that critical steady states disappear below $p = 0.4$ in model A [14], and below $p = 0.5$ in model B [13]. Here we argue that dynamic rules with different correlation times t_c in these models lead to separate prevailing relaxation mechanisms at the edge of the scaling region, which lead to different values of $p^\star$ and to two different universality classes of scaling behavior. In particular, in model A we find that the scaling exponents of large avalanches $\theta(p^\star)$, $\tau_s(p^\star)$, *etc.*, are close to the universality class of parity-conserving (PC) branching and annihilating random walks [20,21], whereas in model B the exponents at $p^\star$ reach the values of the mean-field SOC universality class.

Although the relaxation rules in both model A and model B are complex interplay of the probabilistic critical height and deterministic critical slope rules, we may distinguish two basic type of local branching and annihilating processes that take part to propagate an avalanche in these models. Propagation of an avalanche may stop at a site to which one or two particles drop in time step t, in the following two cases: (1) one particle drop will not continue if the site had height zero, that is "annihilation" $A \to 0$ occurs with probability $1-\rho$, where ρ is the dynamically changing probability that a site has height $h \geq 1$; (2) when two particles drop to a site at time t, the avalanche may not proceed if the diffusion probability p is too low, *i.e.*, $A + A \to 0$ occurs with probability $1 - p$. Note that since number of particles is conserved by the processes in the interior of the pile, "annihilation" means accumulation of particles at a site, which thus will take part in future events, in contrast to the case of chemical reactions, where particles are extinct. When the conditions for toppling are fulfilled, propagation of an avalanche represents a branching process which consists of two steps. A toppled site at time t transfers two particles forward, however, the instability is transferred to its four neighbors, but the site itself can not topple in the next time step. Toppling of an isolated site away from the open boundaries by the critical height (CH) rule makes four neighboring sites as candidates for toppling in the next time step, and if these four sites topple, they make nine new candidates for toppling *etc.*, along the chain $1 \to 4 \to 9 \to 16 \to 25, ...$ Since each toppled site, both initial and triggered sites, topple by two particles, in CH mechanism, this toppling chain represents a reaction $A \to (m+1)A$ with odd number of offsprings $m = 3, 5, 7, 9, ...$ per each initial particle. The same conclusion is true for topplings by the critical slope (CS) rule with two simultaneously unstable slopes. If, however, a site topple by critical slope (CS) rule by dropping one particle along one unstable slope, it will trigger three neighboring sites to topple by CS mechanism, and another toppling chain occurs as $1 \to 3 \to 7 \to ...$, *i.e.*, $m = 2, 4, 6, ...$ offsprings per initial particle.

Diffusion limited branching annihilating random walks (BARW) have been studied by field-theory methods (for a recent review see [22] and references therein). It has been recognized that $d_c = 2$ is the upper critical space dimension, and that BARW with even number of offsprings in $d = 1$ belong to PC universality class, whereas the directed percolation (DP) universality class was found in the case of odd number of offsprings. Two examples of dynamical processes in $1 + 1$ dimension belonging to PC universality class have been studied numerically in references [23, 24]. It should be stressed that in contrast to BARW and DP processes, the present models A and B are dynamical, and thus the propagation rules apply statistically and depend on the history of the state of the system. Recently an analogy between the directed percolation and stochastic dynamical model with critical height rules has been discussed in reference [25].

In model B, short correlation time makes the relaxation at a site less effective with decreasing p, and thus efficient building-up of heights occurs, leading eventually to $\rho(p^\star) \approx 1$ (a transverse section of the pile in model B at $p^\star$ is given in Fig. 6 (bottom)). Therefore, when an instability starts, it may trigger a mixture of branching processes described above, making an instability transferred back and forth on two-dimensional lattice and evolving in time. Fractal dimension associated with the mass of avalanches at the edge of scaling region was found to be $D_n(p^\star) \approx 2$ (see inset to Fig. 5). Thus an avalanche appears to be compact in 2-dimensional space and, since next toppled sites are neighbors in time ($t_c = 1$), it represents a connected object in $(2 + 1)$-dimensions. Starting an instability in *full* lattice, *i.e.*, with no threshold condition, will trigger an avalanche which propagates as a directed percolation cluster in 3-dimensions, until eventually too many sites will have heights zero and the avalanche will stop. Thus $p^\star$ should coincide with the site-directed percolation threshold on simple cubic lattice $p_c^{SDP} = 0.435$ [26]. Mass of avalanche is defined as the number of particles that slide during an avalanche, and thus it is equivalent to number of branchings. Therefore, since for $p = p^\star$ the effective dimension $D_n(p)$ reaches the upper critical

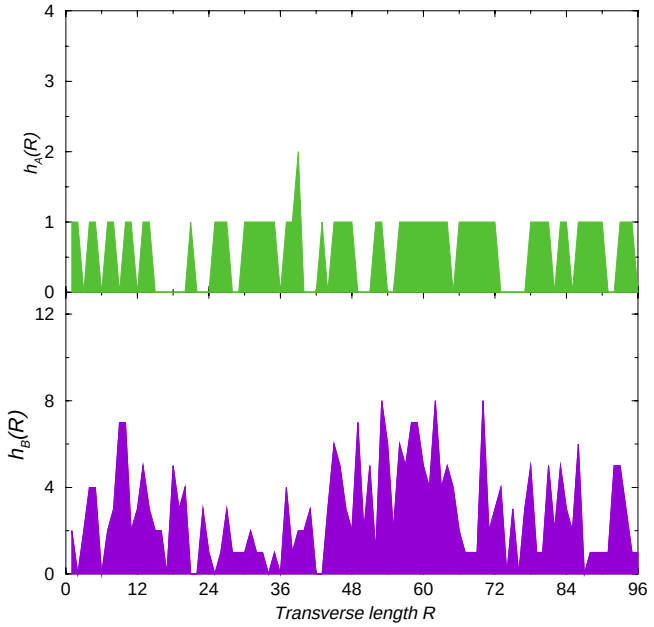

Fig. 6. Transverse section of the pile at distance $\ell = 48$ from the top of pile for $p = 0.435$ in model B (below), and for $p = 0.382$ in model A (top).

Table 1. Critical exponents at $p = 0.4$ in models A and B, and for parity-conserving (PC), and mean-field universality classes (MF-SOC).

E–M	model A	PC	model B	MF-SOC
θ	0.25	2/7	0.78	3/4
z	1.13	8/7	1.33	4/3
$\tau_s - 1$	0.21	2/9	0.68	0.66
$\tau_n - 1$	0.19	—	0.52	1/2
χ	0.05	—	0.18	?

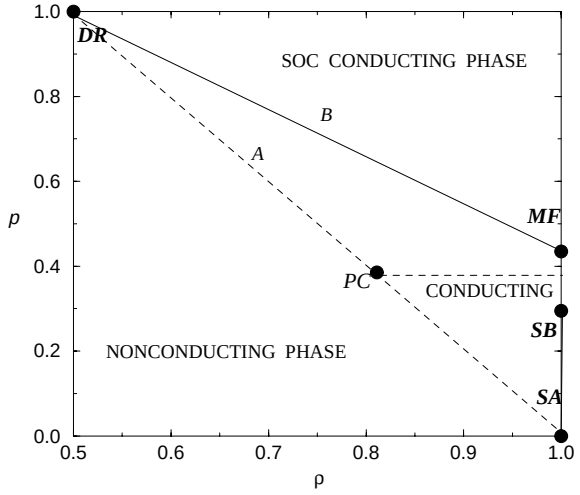

Fig. 7. Schematic phase diagram in (ρ, p) plane. Phase boundaries for model A (dashed lines) and for model B (solid lines).

dimension of BARW, we may expect mean-field universality class for the scaling behavior of avalanches. Our numerical results listed in Table 1 confirm this conclusion. A schematic phase diagram is shown in Figure 7.

The situation is different in model A (*cf.* Fig. 1), where decreasing diffusion probability p an avalanche is either extinct quickly (short avalanches), or lives much longer (large avalanches) with large separation times [14]. In turn, this leads to the efficient topplings at each affected site due to many attempts within correlation time $t_c \gg 1$. In the resulting steady state most of the sites have heights $h < h_c$ (*cf.* Fig. 6 (top)). Therefore, only toppling by CH rule takes place and threshold condition is still active, in contrast to model B. In model A a toppled site (i, j) at time t may trigger topplings at time $t+1$ at three neighboring sites, since the site toppled at $t-1$ time step will not fulfill the threshold condition $(h \geq 2)$ at time $t+1$. It turns that among three neighbors less than two sites topple in the average, therefore leading to a chain of toppled sites with few branches, which is embedded in $(2+1)$-dimensional space-time. However, affected sites which do not topple due to low probability p at first attempt may topple in later time steps before the avalanche dies off, thus starting a new chain. The avalanche is made of set of such chains, and has the fractal dimension $D_n = 1.48$. We believe that this effectively low dimensional BARW process, although it takes part in $(2+1)$-dimensional space-time, is the reason for PC universality class in model A. Another reason for the occurrence of PC universality class in reaction-diffusion processes might be the existence of more than one symmetric absorbing states, as discussed in [23,27]. The process is reminiscent to bond-directed percolation in 3-dimensional simple cubic lattice, thus we also expect that $p^\star \leq p_c^{BDP} = 0.382$ [26]. In the phase diagram in Figure 7 phase boundaries for model A (dashed lines) separate reactive phase from the critical and noncritical absorbing phases.

In the phase diagram in Figure 7 phase boundaries for model A (dashed lines) separate nonconducting phase from the conducting critical and noncritical phases. In model B the noncritical conducting phase exists only along the line $\rho = 1$ below MF point, and a finite slope occurs *via* a phase transition at SB point [13]. On the other hand, in model A our results suggest that noncritical steady states occupy a finite region close to the right corner, and that a finite slope occurs asymptotically at $p = 0$, $\rho = 1$. Further analysis is necessary in order to find precise location of the PC point and the nature of phase transition between critical and noncritical conducting states. Along the phase boundaries between the points PC and DR, and between MF and DR, we have the nonuniversal criticality of model A and model B, respectively, discussed in the present work. The point marked by DR at $\rho = 0.5$, $p = 1$ corresponds to the universal SOC of Dhar-Ramaswamy model.

Sets of the exponents for $p = 0.4$ are summarized in Table 1. Exponents in the model B at this value of p are estimated from the straight sections of lines in the subcritical region for smaller lattice size $L = 128$. Value of the exponent τ_s is taken from reference [13]. For comparison, shown are also the numerical values of the exponents for PC universality class, from reference [21], and mean-field self-organized criticality exponents, from reference [28]. Note that our exponent θ corresponds to the survival probability distribution exponent δ in reference [21], and $z \equiv 2\nu_\perp/\nu_\parallel$ and that the scaling relation $\tau_s - 1 = \theta/(\theta+1)$ holds. The exponents τ_n for mass of avalanche and roughness exponent χ are unique for granular piles, and can not be defined in models of chemical reactions or damage spreading, considered in references [23,24]. We estimate roughness exponent χ from the contour of several transverse sections of the pile (two examples are given Fig. 6). For instance, by using box counting method we find the fractal dimension of the contour curve in model B, as $d_f = 1.179 - 1.183$, and using the expression $\chi = d_f - 1$ leads to the value listed in Table 1.

5 Conclusions

We have shown that sandpile automata with mixed relaxation rules of stochastic diffusion and deterministic branching processes are capable of describing nonunuiversality of the self-organized critical states and a loss of scaling at a critical value of the control parameter, in a qualitative agreement with observed behavior in natural and laboratory granular flow. Differences in the relaxation rules due to internal correlation time lead to distinct dynamic critical states. In particular, unlimited (within lifetime of an avalanche) correlation time t_c in model A leads to a multifractal scaling behavior and scaling exponents of large avalanches *decrease* with decreasing values of the control parameter p. On the other hand, finite correlation time $t_c = 1$ in model B leads to *increase*

of the scaling exponents with decreasing p, and to finite-size scaling properties of avalanches in the entire scaling region $p^\star \leq p < 1$. At the edge of the critical region at $p^\star$, dominating relaxation mechanisms of modulo two conserving branching processes and effectively low dimensionality of the processes, lead to criticality in the parity conserving universality class in model A. In model B building up of a global slope appears to be dominant on top of the above branching processes, which thus appear to have the effective dimension which exceeds the upper critical dimension of BARW, and thus mean-field scaling exponents. It should be stressed that the numerical values of the exponents listed in Table 1 prove the closeness of these universality classes within numerical error bars, which we estimate as 0.03. Value of the exponent $\tau_n = 1.66$ in mean-field models is known only numerically [28], whereas in branching processes, which are equivalent to sandpiles with a fixed number of grains per toppled site, there is the equality $\tau_n = \tau_s = 3/2$. Study of the details of the dynamic phase transition in these models, *e.g.*, in terms of the order parameter and its fluctuations, is left out of the present paper (see, Ref. [13] for appearance of finite slope at SB point in model B). However, due to scaling relations among various exponents at the transition, the observed different universality classes of avalanche statistics at $p^\star$ indicate that the exponents of the order parameter β and correlation length $\nu_\parallel$ should belong to two distinct universality classes of the dynamic phase transitions in these models. Our results suggest that although basic relaxation rules in laboratory granular piles and natural landslides might be the same, details of actual implementation of these rules such as variation of control parameter *during* the course of an avalanche might lead to entirely different critical states.

This work was supported by the Ministry of Science and Technology of the Republic of Slovenia. I would like to thank Uwe Täuber for helpful discussions.

References

1. P. Bak, *How Nature Works* (Copernicus Springer-Verlag, New York, 1996).
2. H.M. Jeager, C.-H. Liu, S.R. Nagel, Phys. Rev. Lett. **62**, 40 (1989).
3. G.A. Held, D.H. Solina, D.T. Keane, W.J. Haag, P.M. Horn, G. Grinstein, Phys. Rev. Lett. **65**, 1120 (1990).
4. J. Rosendahl, M. Vekić, J.E. Rutledge, Phys. Rev. Lett. **73**, 537 (1994).
5. M. Bretz, J.B. Cunningham, L.P. Kurczynski, F. Nori, Phys. Rev. Lett. **69**, 2431 (1992).
6. V. Frette, K. Christensen, A. Malte-Sørensen, J. Feder, T. Jøssang, P. Meaking, Nature (London) **379**, 49 (1996).
7. D.A. Noever, Phys. Rev. E **47**, 724 (1993).
8. J.D. Pelletier, D. Malamud, T. Blodget, D.L. Turcotte, `e-print`, `physics/9705035`.
9. K. Christensen, A. Corral, V. Frette, J. Feder, T. Jøssang, Phys. Rev. Lett. **77**, 107 (1996).
10. C.P.C. Prado, Z. Olami, Phys. Rev. A **45**, 665 (1992).
11. B. Tadić, R. Ramaswamy, Physica A **224**, 188 (1996).
12. L.N. Amaral, K.B. Lauritsen, Phys. Rev. E **56**, 231 (1997).
13. S. Lübeck, B. Tadić, K.D. Usadel, Phys. Rev. E **53**, 2182 (1996).
14. B. Tadić, Phys. Rev. E **57**, 4375 (1998).
15. D.L. Turcotte (unpublished).
16. J.D. Pelletier, `e-print`, `physics/970533`.
17. R. Pastor-Satorras, D.H. Rothman, Phys. Rev. Lett. **80**, 4349 (1998).
18. D. Dhar, R. Ramaswamy, Phys. Rev. Lett. **63**, 1659 (1989).
19. I. Jensen, Phys. Rev. Lett. **77**, 4988 (1996).
20. H. Takayasu, A.Yu. Tretyakov, Phys. Rev. Lett. **68**, 3060 (1992).
21. I. Jensen, Phys. Rev. E **50**, 3623 (1994).
22. J.L. Cardy, U.C. Täuber, J. Stat. Phys. **90**, 1 (1998).
23. M.H. Kim, H. Park, Phys. Rev. Lett. **73**, 2579 (1994).
24. H. Hinrichen, E. Domany, `e-preprint`, `cond-mat/9701011`.
25. B. Tadić, D. Dhar, Phys. Rev. Lett. **79**, 1519 (1997).
26. P. Grassberger, J. Phys. A **22**, 3873 (1989).
27. R.A. Monetti, `e-print`, `cond-mat/9712301`.
28. B. Tadić, R. Ramaswamy, Phys. Rev. E **54**, 3157 (1996).